minerals

Article

Genesis of the Late Cretaceous Longquanzhan Gold Deposit in the Central Tan-Lu Fault Zone, Shandong Province, China: Constraints from Noble Gas and Sulfur Isotopes

Chuanpeng Liu [1,2], Wenjie Shi [3,*], Junhao Wei [3], Huan Li [3], Aiping Feng [1,2], Jun Deng [1,2], Yonglin Yao [1], Jiantai Zhang [1] and Jun Tan [3]

1 The 7th Institute of Geology & Mineral Exploration of Shandong Province, Linyi 276006, China; liuchuanpeng666@163.com (C.L.); 13668697257@139.com (A.F.); sdqydengjun@126.com (J.D.); yaoyl86@163.com (Y.Y.); jiantai26@126.com (J.Z.)
2 Shandong Key Laboratory of Diamond Mineralization Mechanism and Exploration, Linyi 276006, China
3 School of Earth Resources, China University of Geosciences, Wuhan 430074, China; junhaow@163.com (J.W.); lihuanzd@cug.edu.cn (H.L.); tanjun@cug.edu.cn (J.T.)
* Correspondence: shiwenjie@cug.edu.cn

Abstract: The Longquanzhan deposit is one of the largest gold deposits in the Yi-Shu fault zone (central section of the Tan-Lu fault zone) in Shandong Province, China. It is an altered-rock type gold deposit in which ore bodies mainly occur at the contact zone between the overlying Cretaceous rocks and the underlying Neoarchean gneissic monzogranite. Shi et al. reported that this deposit formed at 96 ± 2 Ma using pyrite Rb–Sr dating method and represents a new gold mineralization event in the Shandong Province in 2014. In this paper, we present new He–Ar–S isotopic compositions to further decipher the sources of fluids responsible for the Longquanzhan gold mineralization. The results show that the δ^{34}S values of pyrites vary between 0.9‰ and 4.4‰ with an average of 2.3‰. Inclusion-trapped fluids in ore sulfides have ^{3}He/^{4}He and ^{40}Ar/^{36}Ar ratios of 0.14–0.78 Ra and 482–1811, respectively. These isotopic data indicate that the ore fluids are derived from a magmatic source, which is dominated by crustal components with minor mantle contribution. Air-saturated water may be also involved in the hydrothermal system during the magmatic fluids ascending or at the shallow deposit site. We suggest that the crust-mantle mixing signature of the Longquanzhan gold deposit is genetically related to the Late Cretaceous lithospheric thinning along the Tan-Lu fault zone, which triggers constantly uplifting of the asthenosphere surface and persistent ascending of the isotherm plane to form the gold mineralization-related crustal level magma sources. This genetic model can be applied, to some extent, to explain the ore genesis of other deposits near or within the Tan-Lu fault belt.

Keywords: noble gas isotope; ore-forming fluid; gold deposit; Tan-Lu fault zone; Shandong

Citation: Liu, C.; Shi, W.; Wei, J.; Li, H.; Feng, A.; Deng, J.; Yao, Y.; Zhang, J.; Tan, J. Genesis of the Late Cretaceous Longquanzhan Gold Deposit in the Central Tan-Lu Fault Zone, Shandong Province, China: Constraints from Noble Gas and Sulfur Isotopes. *Minerals* **2021**, *11*, 250. https://doi.org/10.3390/min11030250

Received: 1 December 2020
Accepted: 24 February 2021
Published: 28 February 2021

1. Introduction

The Shandong Province situated in the southeastern margin of the North China Craton (NCC) is the largest gold-producing region in China. It has proven reserves exceeding 5000 tons (t) Au and more than 150 active gold mines produce at least 30 t of gold per year [1–3]. This gold province is separated tectonically by the Yi-Shu fault zone (central part of the Tan-Lu fault zone in the Shandong Province) into two distinct domains, namely the Luxi to the west and the Jiaodong to the east (Figure 1) [4,5]. A variety of studies has been conducted on these gold deposits over the past decades and have revealed that gold metallogeny across the Shandong Province contrasts markedly, i.e., by mineralization type (altered-rock type and quartz-vein type vs. crypto explosive breccia type and skarn type), mineralization age (ca. 120–125 Ma vs. 180–170, 133–128, and 98–94 Ma), and mantle dynamics (EMII type vs. EMI type, [1,5,6]). Nevertheless, almost all gold deposits from either the Jiaodong or the Luxi show a clear magmatic affinity for their hydrothermal system as indicated by fluid inclusions and multi-stable and radiogenic isotopes [1,4–7]. This suggests that the ore fluids and, by inference, ore metals were dominantly derived from the coeval magmatism [1,2,4–11]. He–Ar isotopes further suggested that most deposits have mixed sources of both crustal and mantle origin and that the involvement of mantle-derived components was probably related to craton recycling and resultant mantle upwelling [1,2,8–13]. However, the proportion of mantle contributions varies significantly among these deposits and predictably results in the differences between the Jiaodong and the Luxi areas. For example, Liu et al. (2014) found that ore fluids of the Yi'nan gold deposit from the Luxi area were mainly derived from a mixed crust-mantle magmatic source and that the involvement of mantle components in gold mineralization was significantly lower than those from the Jiaodong [4].

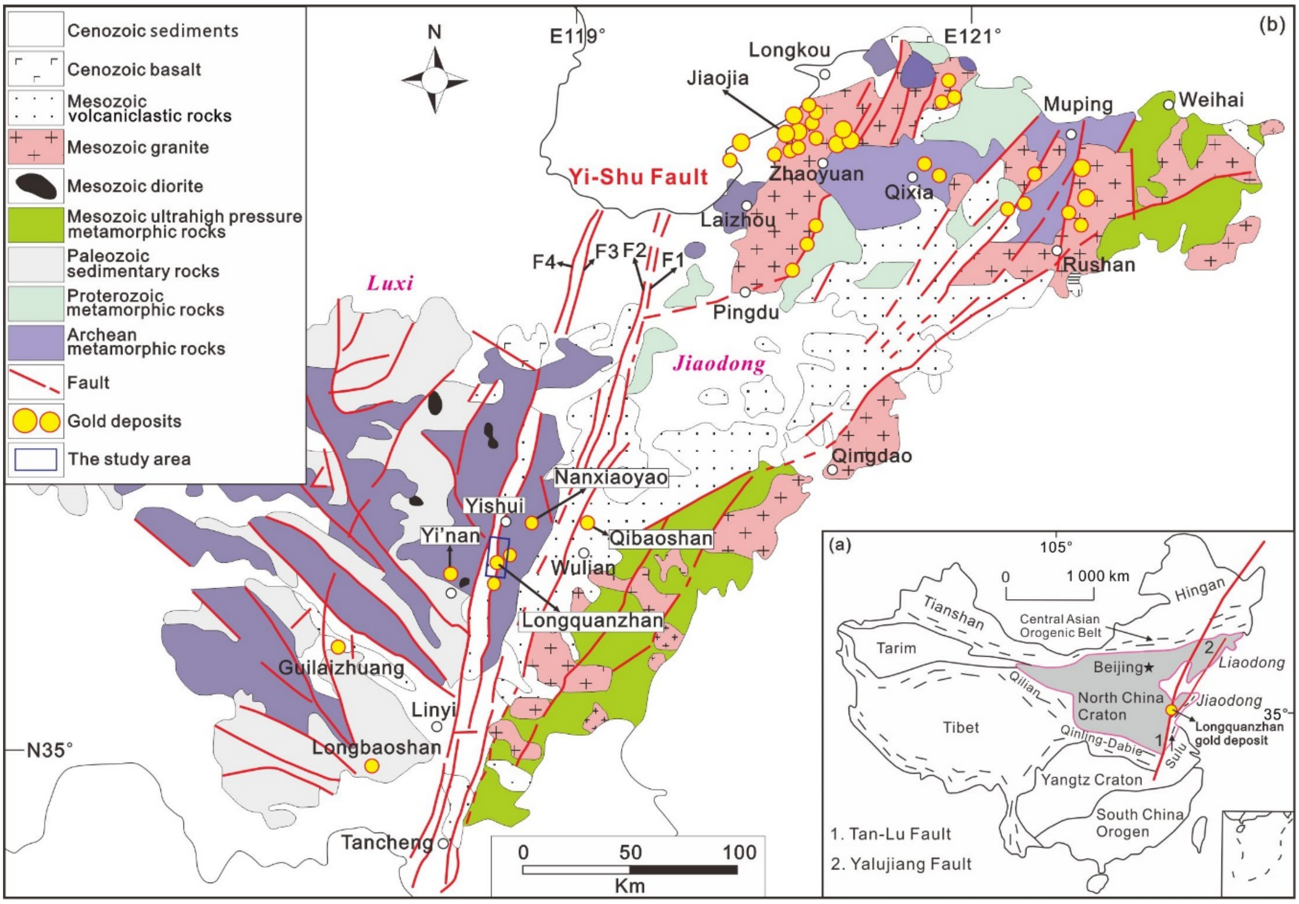

Figure 1. (**a**) Tectonic map illustrating the major tectonic divisions of China (modified from [14]); (**b**) Geological map showing the geology and major deposits of the Shandong Province (modified from [4]). F1: Changyi-Dadian fault, F2: Anqiu-Juxian fault, F3: Yishui-Tangtou fault, F4: Tangwu-Gegou fault.

Additionally, the lithospheric thinning during the late Mesozoic has been identified beneath the Shandong Province [15,16]. The Early Cretaceous magma upwelling was consistent with the peak of gold mineralization in the Shandong and is considered to provide abundant ore-forming materials [1,8–11]. This is evidenced by the fact that numerous intermediate-mafic dikes displaying clear crust-mantle mixing character are temporally and spatially associated with gold mineralization [12,17–20]. Recently, Shi et al. (2014) conducted a pyrite Rb–Sr dating study on the Longquanzhan gold deposit, the largest gold deposit in the Yi-Shu metallogenic belt, and yielded an isochron age of 96 ± 2 Ma [21]. This mineralization age revealed a previously unrecognized gold mineralization event in the Shandong Province, which is almost coeval with the Late Cretaceous magma and volcanic activities in the Tan-Lu fault zone [15,22]. However, the genesis and tectonic setting of the Longquanzhan and other gold deposits in the Yi-Shu fault zone has not yet been well constrained, as well as the implications for regional gold mineralization.

The Longquanzhan gold deposit, therefore, is considered as a valuable case-study in the Yi-Shu fault zone. Previous studies have unilaterally described the geological characteristics of this deposit, lacking a systematic research of geochemical isotopes on the ore-forming system [21]. Additionally, few studies have been conducted comparing the Longquanzhan deposit with other gold deposits across the Yi-Shu fault zone (i.e., from the Luxi to the Jiaodong). In this study, noble gas and sulfur isotopes of pyrites in the main gold mineralization stage are measured to trace the sources of ore-forming fluids and metals for the Longquanzhan deposit and to further constrain the origin of Late Cretaceous gold mineralization event in the Yi-Shu fault zone. The new data are combined with noble gas obtained for the Yi'nan and Qibaoshan gold deposits (Figure 1) and previously published isotopic data for other gold deposits in the Luxi and Jiaodong in order to discuss gold mineralization variations across the Shandong Province.

2. Geological Background

The NNE striking Tan-Lu fault zone is trans-lithospheric (about 80 km deep) and extends up to 2400 km along the eastern margin of the NCC [23]. It can be divided into three sections of which the middle one within the Shandong Province is called the Yi-Shu fault zone. From east to west, the Yi-Shu fault zone consists of four main sub-faults: the Changyi-Dadian (F1), the Anqiu-Juxian (F2), the Yishui-Tangtou (F3), and the Tangwu-Gegou (F4) (Figure 1) [23]. The Yi-Shu fault zone crosscuts the Shandong Province and separates it into two parts, namely the Luxi to the west and the Jiaodong to the east (Figure 1). The evolution of the Yi-Shu fault zone controlled the distribution of late Mesozoic fault activity and magmatism, formation of the sedimentary basin, and gold mineralization within the fault zone and vicinity [1,5,20,24,25].

The Precambrian basement in the Yi-Shu fault zone is composed of the Mesoarchean Yishui Group, the Neoarchean Taishan Group, and the Neoproterozoic Tumen Group (Figure 2) [26]. The Yishui Group is composed of granulite and amphibolite with minor quartzite, dated from 2986 to 2997 Ma by whole-rock Sm–Nd method [27]. The Taishan Group consists of amphibolite and biotite granulite with minor TTG gneiss, which were metamorphosed in amphibolite and greenschist facies. It contains the succession made up of the Yanlingguan, the Shancaoyu, and the Liuhang Formations. Wang et al. (2012) reported zircon SHRIMP U–Pb ages of ca. 2750 to 2700 Ma for the Yanlingguan Formation and of ca. 2560–2530 Ma for the Liuhang Formation [28]. The Tumen Group is composed of shale, sandstone, limestone, and conglomerate. Most of these basement rocks are overlain by the Palaeozoic rocks consisting dominantly of fluvial-clastic rocks and carbonates, with smaller amounts of marine clastic rocks. They include the Changqing, the Jiulong, and the Yuemengou Groups (Figure 2) [24]. The subsequent Mesozoic to Cenozoic strata consist mainly of volcano-sedimentary rocks, which are widely distributed in the Mesozoic basins (Figure 2). Among them, the Cretaceous Dasheng Group and Wangshi Group are mainly composed of continental-lake-phase clastic volcanic rocks, while the Qingshan Group consists of felsic-intermediate compositions of continental volcanic rocks (Figure 2) [29]. The Bamudi Formation within the Qingshan Group can be further distinguished into a potassic type and a sodic type and their corresponding zircon LA-ICP-MS U–Pb dating ages are 124 ± 1 Ma and 106–97 Ma [22,29], respectively. Cenozoic sediments composed of sandstone and breccia locally cover both the Precambrian and the Mesozoic rocks. Ultra-high pressure (UHP) metamorphic rocks outcrop widely adjacent to the southeast section of the Yi-Shu fault zone. They are dominated by eclogite, garnet peridotite, garnet pyroxenite, jadeite quartzite, and garnet gneiss, with ages of 243–228 Ma dated by zircon SHRIMP U–Pb method [30].

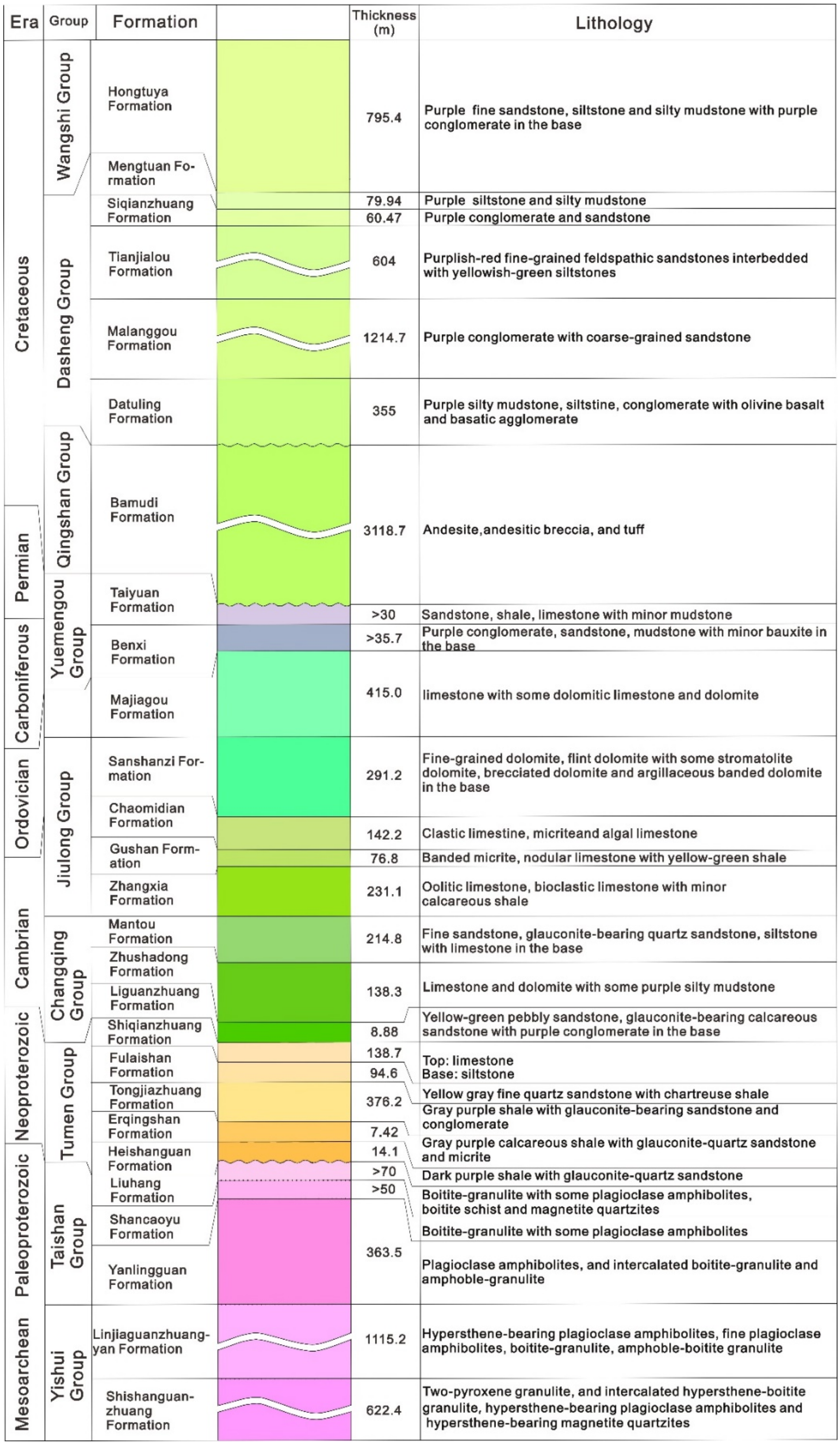

Figure 2. Summarized stratigraphic column for the Yishui region in the central Shandong Province (modified from [26]).

The Yi-Shu fault zone is characterized by voluminous intrusive and volcanic rocks and intermediate-mafic dikes (Figures 1–3). They have two main formation episodes, Neoarchean to Paleoproterozoic and Mesozoic. The former is represented by the Yishui and Dashan intrusions and consists mainly of trondhjemite, tonalite granodiorite, monzogranite, and alkali feldspar granite (2706–2490 Ma) [31–33]. These ancient rocks are associated with the most important crust-forming event in the Jiaodong Terrain [34]. The Mesozoic intrusions are unexposed and dominated by small-scale felsic granite porphyry (Figure 3). The volcanic rocks consist mainly of trachybasalt, latite, trachyte and rhyolite flows, and pyroclastic rocks, the same as the components of the Qingshan Formation. A suite of NE and NNE fault-hosted intermediate to mafic dikes intrude into the granitoids and Precambrian basement rocks (Figure 3). They consist mainly of dolerite, gabbro, lamprophyre, and diorite and exhibit crust-mantle interaction signatures [35,36].

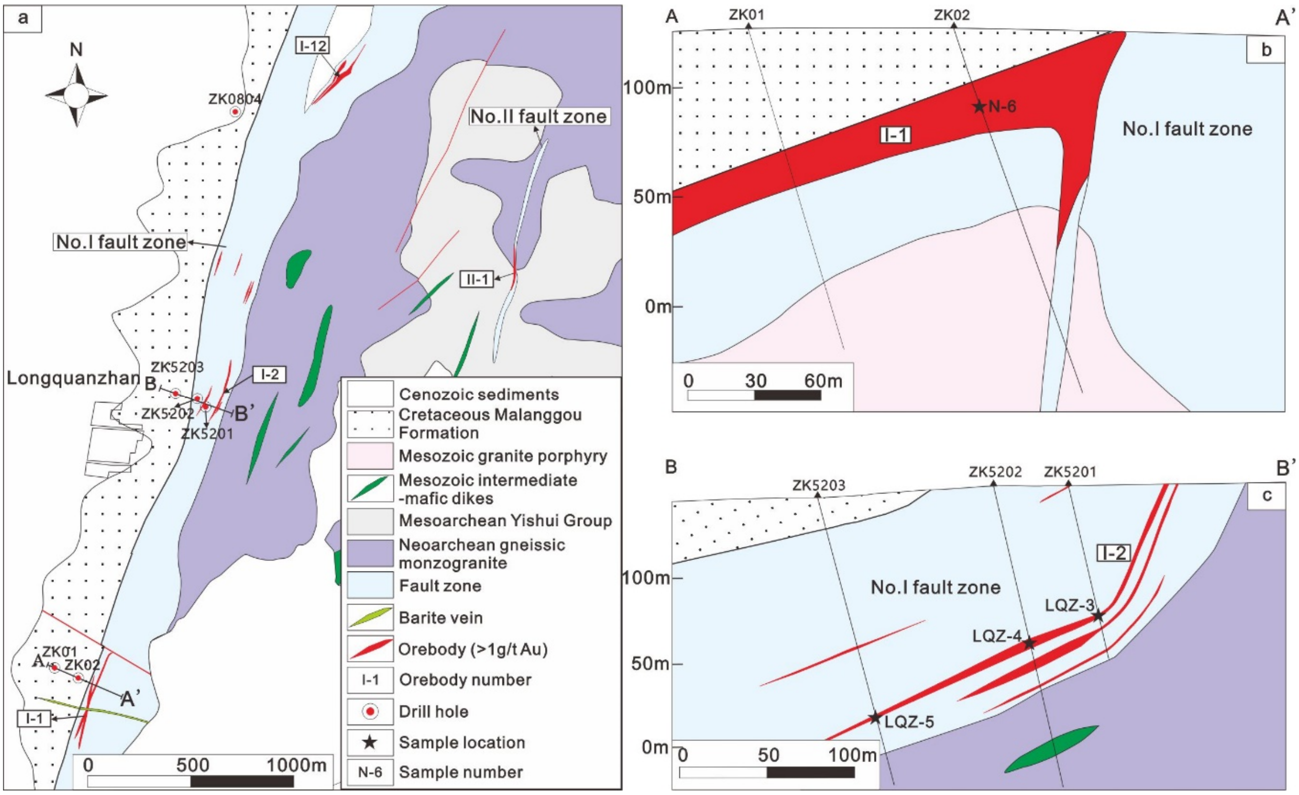

Figure 3. (**a**) Geological map of the Longquanzhan gold deposit; (**b**) geological profiles A-A'; and (**c**) geological profiles B-B'.

3. Deposit Geology

The Longquanzhan gold deposit is located approximately 12 km south of the Yishui County (Figure 1). Five lithologies can be identified in the district (Figure 3a): (1) Mesoarchean Yishui Group, (2) Neoarchean gneissic monzogranite, (3) Mesozoic granite porphyry and intermediate-mafic dikes, (4) Cretaceous sedimentary rocks, and (5) Cenozoic sediments. The Yishui Group consists of granulite intercalated with plagioclase amphibolite and magnetite quartzite, with metamorphic grade ranging from upper amphibolite to granulite facies [27]. The Yishui monzogranite has undergone intermediate deformation and is the major wall rock of gold ore bodies. The Mesozoic intermediate-mafic dikes are mainly composed of gabbro, diorite, and diabase. Some dikes themselves were mineralized and are thus interpreted to have intruded before the ore formation. The Mesozoic granite porphyry occurs in a few small outcrops but is common in underground workings or drill cores (Figure 3b). These are present either in proximal ore veins or crosscut by mineralized zones. The Cretaceous sedimentary rocks constitute the Malanggou Formation, which discordantly overlies the Archaean rocks and is composed of purplish-red fine-grained feldspathic sandstones interbedded with yellowish-green siltstones (Figure 4a,b). The Cenozoic sediments are composed of sandstone and mudstone and locally cover the ancient rocks.

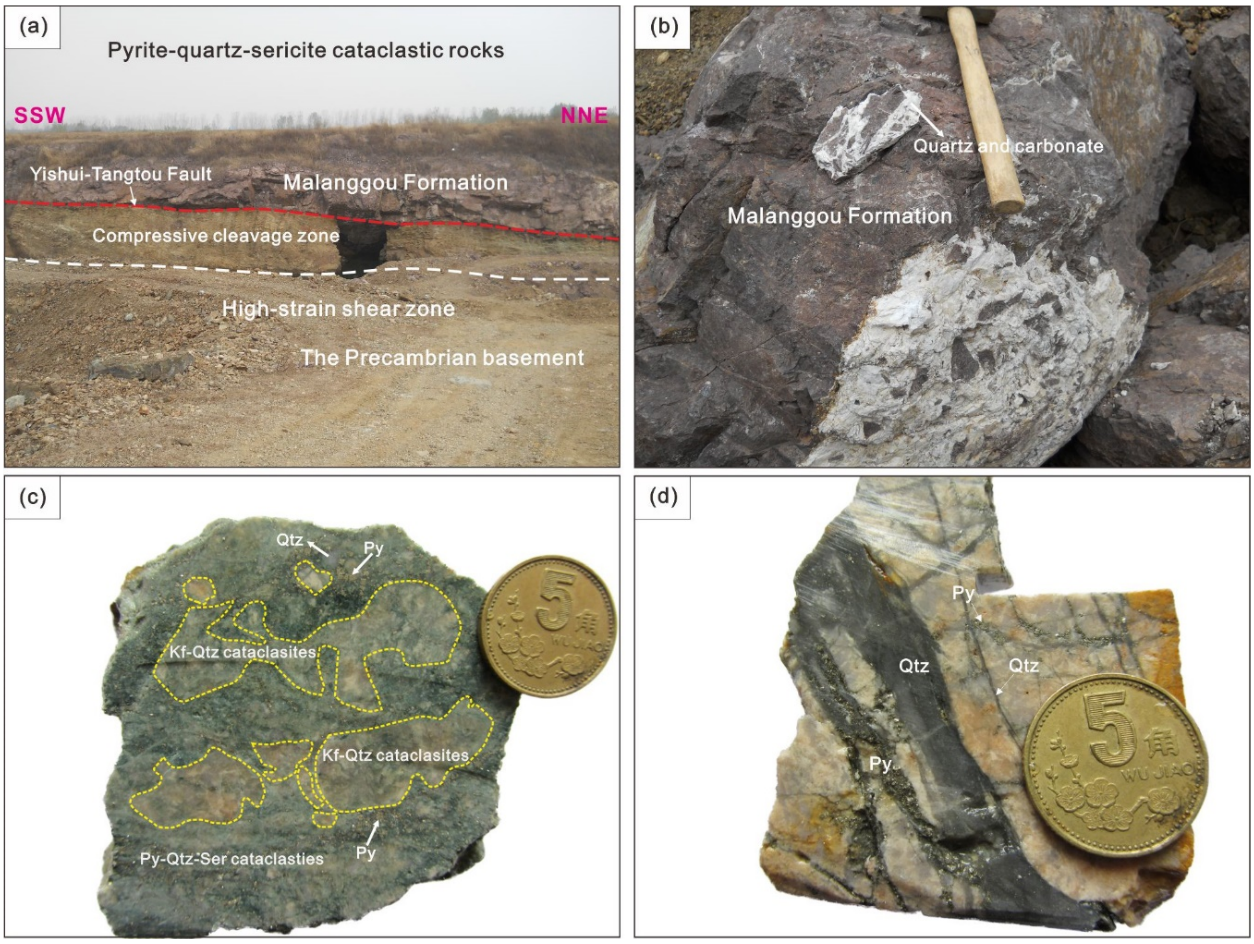

Figure 4. Geology, ore type, and mineralization features of the Longquanzhan gold deposit. (**a**) Panoramic view of the Yishui-Tangtou fault; (**b**) breccias of the Cretaceous Malanggou Formation, with cementing materials of quartz and carbonate; (**c**) altered rock-type ores with early K-feldspar overprinted by late pyrite, sericite, and quartz; and (**d**) gold-bearing quartz vein/veinlets within the footwall gneissic monzogranite. Abbreviations: Py =pyrite; Ser = sericite; Qtz = quartz; Kf = K-feldspar.

The ore bodies are controlled by the Yishui-Tangtou fault, with the Malanggou Formation in the hanging wall and the Neoarchaean Yishui monzogranite in the footwall (Figure 3b,c). Granulite and amphibolite of the Yishui Group occur as enclaves in the monzogranite and locally host ore bodies. However, the main ore host rocks are the gneissic monzogranite. This fault, with a length of ca. 13 km, strikes approximately SSW 190°–205° with a dip of 35°–70° NWW (Figure 4a). Two subordinate NNE-trending brittle-ductile fault zones (No. I and II) in the footwall of the Yishui-Tangtou fault plane are developed. No. I fault extending more than 11 km, with a width of 80–460 m, is the main ore-controlled structure, which hosts roughly 95% of the total reserves of the deposit (Figure 3). A total of twelve ore bodies are delineated within the No. I fault; they mainly form lodes, lenses, and stringers with a strike of SSW 195°–215°and a dip angle of 30°–55° NWW (Figure 3a), and have lengths of 200–600 m and widths of 0.83–40 m. No. II fault is only 2.3 km in length and 5–60 in width and hosts two small ore bodies (Figure 3a). Two types of mineralization are identified: altered rock-type and auriferous quartz vein/veinlet-type (Figure 4c,d). The former is predominant in the district and largely composed of disseminated, fine-grained to medium-grained, pyrite, and quartz-sericite-pyrite stockworks. Auriferous quartz vein/veinlets are found locally in the alteration halos. The ores have Au grades from 1.08 to 92.29 g/t (average ca. 2.62 g/t) and reserves of approximately 6 t Au [21].

Hydrothermal alteration is well developed in the Longquanzhan gold deposit, which is mostly restricted to 0.5 to 5 m wide zones around ore bodies. The main alteration types include potassium feldspathization, chloritization, sericitization, silicification, and carbonatization. Although there is no obvious zonation of the alteration, quartz, K-feldspar, and sericite are commonly developed within mineralized veins, whereas chlorite and carbonate mostly occur away from ore bodies. Potassium feldspathization, pre-dating the gold and characterized by K-feldspar overprinting plagioclase or formed around the pre-existed K-feldspar, is often restricted to mineralized veins (Figure 4c), or extends a few meters from the gold ore bodies. Chlorite is often formed by replacing wall-rock biotite or hornblende (Figure 5a). Sericite, the most abundant alteration product following quartz, is formed via replacement of wall-rock plagioclase or pre-existing hydrothermal K-feldspar (Figure 5b). As ore-related alteration phases, sericite and quartz are usually in textural equilibration with sulfides (Figure 5b,c). The carbonation overlaps other alterations and mainly occurs during late mineralization stage (Figure 5d). Alteration type and intensity usually change with lithologies: quartz, sericite, and K-feldspar are commonly developed in gneissic monzogranitic rocks, whereas chlorite and carbonate are mainly restricted to granulite or amphibolite wall rocks.

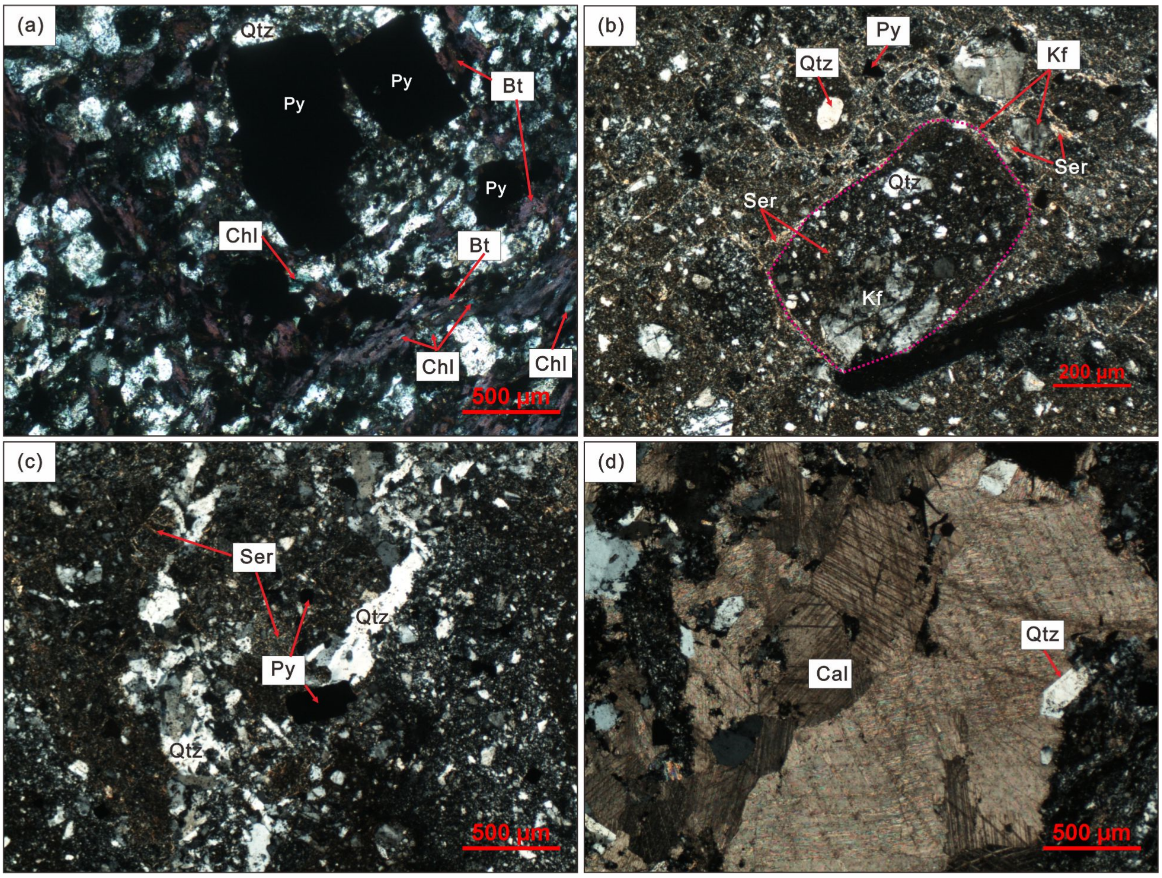

Figure 5. Photomicrographs of hydrothermal alterations of the Longquanzhan gold deposit. (**a**) chloritization, silicification and pyritization in amphibolite wall rocks; (**b**) pyritization, sericitization, and silicification in monzogranite; (**c**) sericite alteration assemblages are crosscut by a quartz-pyrite vein in monzogranite; and (**d**) calcite and quartz in carbonation stage in monzogranite. Abbreviations: Py =pyrite; Ser = sericite; Qtz = quartz; Kf = K-feldspar; Pl = Plagioclase; Chl = chlorite; Bt = biotite; Cal = calcite.

The sulfides account for 30 to 60 vol. % of all minerals and are dominated by pyrite with lesser amounts of chalcopyrite, galena, and sphalerite (Figures 6 and 7). They typically occur as densely disseminated aggregates and irregular veins intergrown with quartz.

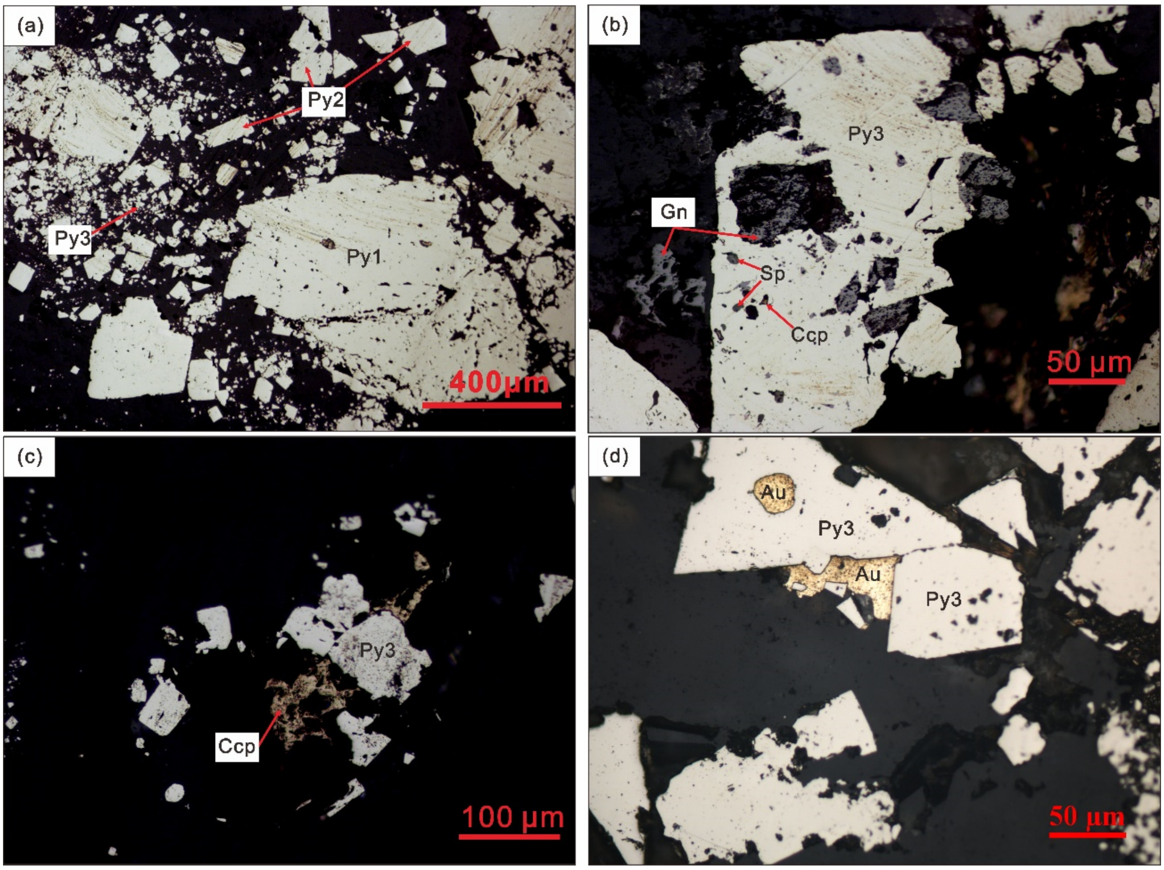

Figure 6. Representative photomicrographs showing the major metallic minerals of the Longquanzhan gold deposit. (**a**) Coarse to fine-grained, subhedral to anhedral pyrite (Py1, Py2, and Py3); (**b**) medium to fine-grained, subhedral pyrite (Py3) intergrown with chalcopyrite, galena, and sphalerite; (**c**) pyrite (Py3) intergrown with chalcopyrite in gold-quartz-polymetallic sulfide stage; (**d**) gold inclusions in the third pyrite stage and fillings between pyrite and quartz. Abbreviations: Py = pyrite; Ccp = chalcopyrite; Gn = galena; Sp = sphalerite; Au =gold.

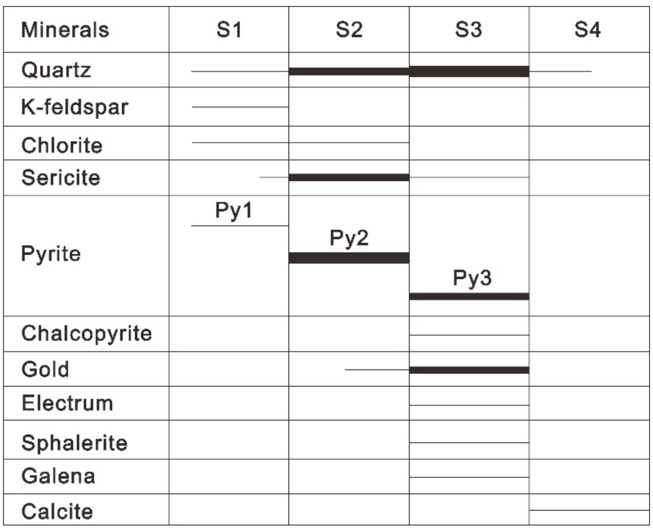

Figure 7. Paragenetic sequence of main minerals in the Longquanzhan gold deposit.

Four stages of hydrothermal alteration and mineralization have been recognized based on cross-cutting relationships of veinlets, ore structures and textures, and mineral paragenetic assemblages (Figure 7). They, from early to late, are described below:

(1) Quartz-pyrite stage. This is represented by an assemblage of white quartz, coarse-grained pyrite, chlorite, and K-feldspar (Figure 5a–c). The pyrite (Py1) grain size often clusters within a narrow range of 1–3 mm, euhedral to subhedral, and is essentially barren of gold (Figure 6a).

(2) Quartz-sericite-pyrite stage. Sericite occurs as small scaly aggregates (Figure 5b,c), either replacing plagioclase in wall rocks or occurring as veinlets surrounding porphyroblasts (Figure 5b), and is accompanied by fine-grained quartz and minor pyrite. In this stage, the size of pyrite (Py2) grains is normally in the range of 0.5–1 mm (Figure 6a).

(3) Gold-quartz-polymetallic sulfide stage. The minerals of this stage are characterized by volumetrically dominant pyrite and quartz, with subordinate chalcopyrite, galena, sphalerite, electrum, and native gold (Figure 6b–d). Gold occurs mostly in the form of small grains of native Au, either as inclusions in other minerals or as fillings of small fissures (Figure 6d). Generally, relatively intense gold mineralization occurs in the segments where quartz and sulfides are well developed. In this stage, the pyrite (Py3) grain size often clusters around 0.05–0.1 mm (Figure 6a–d).

(4) Carbonation stage. This stage is the last mineralization stage, and the carbonate minerals, dominantly calcite, often occur as veinlet-shaped grains (Figure 5d).

4. Sampling and Analytical Methods

4.1. Sample Description

Four samples from the altered rock-type ore (type I) and five samples from the quartz-veinlet -type ore (type II) were collected from underground mines and drill cores from the Longquanzhan gold deposit for investigation in detail (Table 1). The main ore minerals of the type I and type II ores are pyrite and minor chalcopyrite, galena, sphalerite, electrum, and native gold (Figures 4 and 6). Five pyrite samples of the type I ore and four pyrite samples of the type II ore were selected for noble gas and sulfur isotopic analyses. Previous studies have shown that pyrites were deposited in association with gold from the same fluids in the Shandong gold province, thus noble gas of inclusion-trapped fluid in pyrites and sulfur isotopic compositions of pyrites can be used to trace sources of the mineralizing fluids [1,11,12]. In order to compare the Longquanzhan ore genesis with other gold deposits across the Yi-Shu fault zone, another five pyrite samples from the main mineralization stage of the Yi'nan skarn gold ore and the Qibaoshan cryptoexplosive-breccia-type gold ore were also collected for noble analyses (Table 1). The detailed deposit geology and mineralization features of these two deposits can be referred to [4] and [37], respectively.

Table 1. Sampling locations of ores from the Longquanzhan, Yi'nan, and Qibaoshan gold deposits.

Sample	Sulfide Assemblage	Mining Area	Lithology	Mineralization Stage	Sampling Location
N-6	Py (35%) + Gn (7%) + Sp (5%)	Longquanzhan [1]	Gneissic monzogranite	Gold-quartz-polymetallic sulfide stage	+82 m Drill ZK02
N-9	Py (50%) + Gn (5%) + Sp (5%)	Longquanzhan [1]	Gneissic monzogranite	Gold-quartz-polymetallic sulfide stage	Drill ZK02 SE + 30 m
N-20	Py (60%)	Longquanzhan [1]	Gneissic monzogranite	Quartz-sericite-pyrite stage	Drill ZK02 SE + 90 m
N-22	Py (40%) + Gn (7%) + Sp (3%)	Longquanzhan [2]	Gneissic monzogranite	Gold-quartz-polymetallic sulfide stage	Drill ZK02 SE + 150 m
N-24	Py (40%) + Gn (3%) + Sp (3%)	Longquanzhan [1]	Gneissic monzogranite	Gold-quartz-polymetallic sulfide stage	Drill ZK02 SE + 200 m
LQZ-2	Py (30%) + Gn (6%) + Sp (4%)	Longquanzhan [2]	Amphibolite	Gold-quartz-polymetallic sulfide stage	–157 m Drill No. ZK0804

Table 1. *Cont.*

Sample	Sulfide Assemblage	Mining Area	Lithology	Mineralization Stage	Sampling Location
LQZ-3	Py (20%) + Gn (7%) + Sp (5%)	Longquanzhan [2]	Gneissic monzogranite	Gold-quartz-polymetallic sulfide stage	+63 m Drill No. ZK5201
LQZ-4	Py (40%)	Longquanzhan [2]	Gneissic monzogranite	Quartz-sericite-pyrite stage	+53 m Drill No. ZK5202
LQZ-5	Py (30%) + Gn(5%) + Sp(5%)	Longquanzhan [2]	Gneissic monzogranite	Gold-quartz-polymetallic sulfide stage	0 m Drill No. ZK5203
TJ-2	Py (40%) + Cpy (10%)	Yi'nan [3]	Marble	Quartz-sulfide stage	–130 m Tunnel + CM3
TJ-8	Py (42%) + Cpy (5%)	Yi'nan [3]	Marble	Quartz-sulfide stage	–141 m Drill No.CK99-14
TJ-1	Py (43%) + Cpy (5%)	Yi'nan [3]	Marble	Quartz-sulfide stage	–138 m Drill No.CK92-24
QRSH-8	Py (30%) + Cpy (10%) + Ht (20%)	Qibaoshan [4]	Quartz Dioritic Porphyrite	Gold-quartz-polymetal sulfide stage	–212 m Drill No Zk112-06
QBSH-10	Py (20%) + Cpy (10%) + Ht (5%)	Qibaoshan [4]	Quartz Dioritic Porphyrite	Gold-quartz-polymetal sulfide stage	–52 m Drill No Zk110-02

[1,2] Altered rock-type and auriferous quartz vein/veinlet-type ores from the Longquanzhan gold deposit, respectively; [3] Skarn gold ore from the Yi'nan deposit. The detailed ore geology is described by [4]. [4] Cryptoexplosive-breccia-type gold ore from the Qibaoshan deposit. The detailed ore geology is described by [37]. Mineral abbreviations: Py = Pyrite, Gn = Galena, Sp = sphalerite, Cpy = Chalcopyrite, Ht = Hematite.

4.2. He–Ar Isotope Analyses

Noble gas isotope analyses were performed with an MM5400 gas mass spectrometer (Micromass) at the National Key Laboratory of Gas Geochemistry, Institute of Geology and Geophysics, Chinese Academy of Sciences (Beijing, China). The experiment was conducted at electric currents of It4 = 800 μA and It40 = 200 μA and at a high potential of 9.000 kV. All weighed samples of pyrite for analysis were packed into aluminum foil and shifted to the crucible for gas extraction under high vacuum conditions. When a pressure lower than 1×10^{-5} Pa was attained, the samples were heated at 130 °C for at least 10 h to drive out water vapor [38] and trace gases occurring in cleavage traces or fractures in the crusts. Then, the samples were fused at high temperatures up to 1600 °C, and the released gases were purified through activated charcoal traps at the temperature of liquid nitrogen to separate He and Ar from Ne + Kr + Xe for He and Ar analyses on the mass spectrometer. The minimum heat blanks for the MM5400 mass spectrometer at 1600 °C were ^{4}He = 1.10×10^{-14} mol; ^{20}Ne = 1.82×10^{-14} mol; ^{0}Ar = 6.21×10^{-13} mol; ^{84}Kr = 1.37×10^{-16} mol; and ^{132}Xe = 5.65×10^{-18} mol. The standard for normalizing the analytical results was air in Lanzhou (AIRLZ2003), and the analytical precision for the noble gases isotopic measurements was better than 10%. The detailed sample preparation and measurement procedures followed those in [39].

4.3. Sulfur Isotope Analyses

Sulfur isotope composition was obtained by using a MAT-251EM mass spectrometer at the Stable Isotope Laboratory, Beijing Research Institute of Uranium Geology (Beijing, China). Approximately 20 mg of sulfides were homogenized with 200 mg of Cu_2O and then combusted at 1050–1060 °C for 20 min in a vacuum for a quantitative conversion to sulfur dioxide (SO_2). Sulfur isotope ratios were determined by a conventional off-line method [40]. Data are reported with an accuracy of ±0.2‰ relative to Vienna Canyon Diablo Troilite (V-CDT).

5. Results

5.1. He–Ar Isotopic Compositions

The noble gas isotopic compositions of nine pyrite separates, in combination with five previously published sets of data, are summarized in Table 2 and illustrated in

Figures 8 and 9. The ^{4}He concentrations of pyrite from the Longquanzhan gold deposit range from 0.96 × 10^{-7} to 10.50 × 10^{-7} cm^3 STP/g with an average of 6.20 × 10^{-7} cm^3 STP/g, and the $^{3}He/^{4}He$ ratios are between 0.14 and 0.78 Ra with an average of 0.30 Ra (where Ra is the $^{3}He/^{4}He$ ratio of atmospheric air = 1.39 × 10^{-6}, [41]). The values of ^{40}Ar range between 2.81 × 10^{-7} and 7.99 × 10^{-7} cm^3 STP/g with an average of 5.32 × 10^{-7} cm^3 STP/g. Correspondingly, $^{40}Ar^{*}$ (where $^{40}Ar^{*}$ is the radiogenic ^{40}Ar present, corrected for atmospheric contributions assuming that all ^{36}Ar is atmospheric in origin and an atmospheric $^{40}Ar/^{36}Ar$ of 298, [42]) are between 1.07 and 6.68 × 10^{-7} cc STP/g. The $^{40}Ar/^{36}Ar$ ratios range from 482 to 1811 (average 1078), which are clearly higher than the atmospheric standard value of 298 [42]. By contrast, $^{3}He/^{4}He$ ratios of the Yi'nan and Qibaoshan gold deposits are 0.11–1.12 Ra and 0.19 Ra, but the ranges of $^{40}Ar/^{36}Ar$ are lower, 364–826 and 298–842, respectively (Table 2).

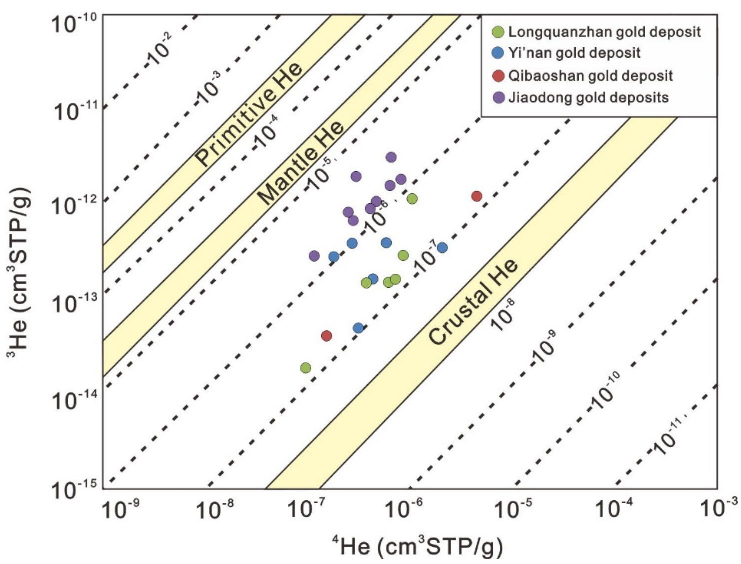

Figure 8. ^{4}He vs. ^{3}He diagram for ore fluid released from pyrite samples in the Longquanzhan, Yi'nan, Qibaoshan, and the Jiadong gold deposits. The He–Ar isotopic data for the typical Jiaodong gold deposits are from [44] and [45]. The He–Ar isotopic data for the Yi'nan gold deposits are from [4]. The $^{3}He/^{4}He$ ratios of the primitive He, mantle He, and crustal He fields are from [41].

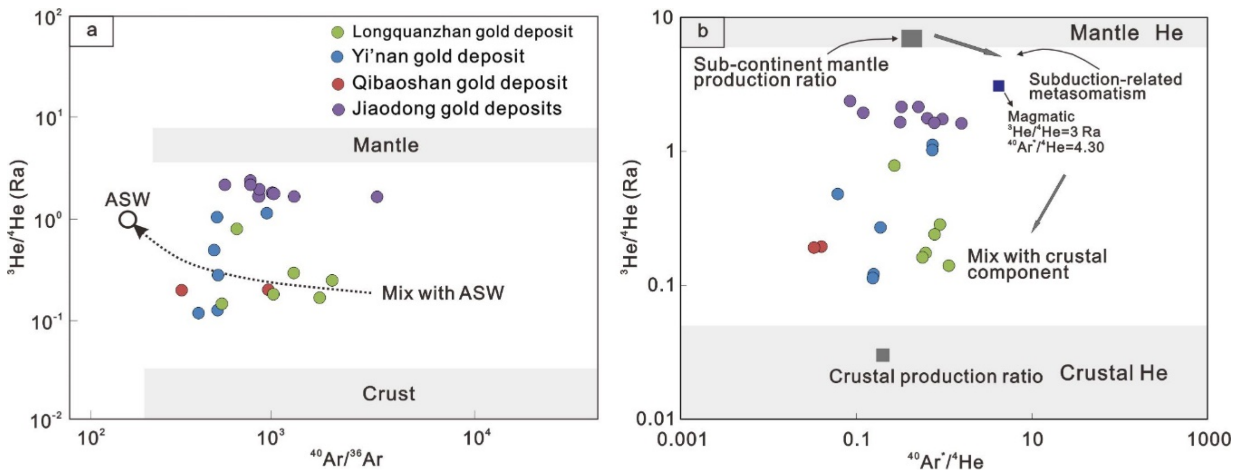

Figure 9. (**a**) R/Ra vs. $^{40}Ar/^{36}Ar$ and (**b**) R/Ra vs. $^{40}Ar^{*}/^{4}He$ plots of inclusion-trapped fluids in pyrite from the Longquanzhan gold deposit and the Luxi-Jiaodong gold ore system. The He–Ar isotopic data for the typical Jiaodong gold deposits are from [44,45]. The magmatic and crustal end-member $^{3}He/^{4}He$ ratios of the Jiaodong area are from [12] and [46], respectively. ASW = atmospheric saturated water (after [47]).

Table 2. He and Ar isotopic compositions of inclusion-trapped fluid in pyrites from the Longquanzhan, Yi'nan, and Qibaoshan gold deposits.

Sample Locations	Sample	Measured Minerals	^{4}He (cm^{3} STP/g) (E^{-7})	^{40}Ar (cm^{3} STP/g) (E^{-7})	^{3}He/^{4}He (Ra)	^{38}Ar/^{36}Ar	^{40}Ar/^{36}Ar	^{40}Ar*/^{4}He	^{40}Ar* (%)	He_{Mantle}(%)	Data Source
Yi'nan gold deposit	LJ-29-2	Py	1.80	2.07	1.12	n.a.	826.0	0.74	64.23	18.45	[4]
	LJ-29-5	Py	5.86	1.10	0.48	n.a.	439.4	0.06	32.75	7.85	
	LJ-29-7	Py	4.33	2.28	0.27	n.a.	460.4	0.19	35.82	4.34	
	TJ-2	Py	20.59	9.16	0.12	0.16	458.0	0.16	35.48	1.85	This study
	TJ-8	Py	3.13	2.56	0.11	0.01	364.1	0.15	18.84	1.72	
	TJ-1	Py	2.73	5.73	1.02	b.d.	454.7	0.74	35.01	16.81	
Qibaoshan gold deposit	QBSH-10	Py	44.94	2.78	0.19	b.d.	842.4	0.04	64.92	3.07	
	QRSH-8	Py	1.53	7.53	0.19	0.22	297.5	0.03	0.67	3.02	
Longquanzhan gold deposit	LQZ-2	Py	10.50	5.85	0.78	b.d.	577.1	0.27	48.80	12.85	
	LQZ-3	Py	6.18	5.69	0.17	0.19	893.6	0.62	66.93	2.74	
	LQZ-4	Py	3.74	4.52	0.28	0.19	1142.4	0.90	74.13	4.57	
	LQZ-5	Py	7.21	5.05	0.16	0.19	1559.1	0.57	81.05	2.52	
	Zk5201-H64	Py	8.59	7.99	0.24	n.a.	1811.0	0.78	83.68	3.84	[43]
	Sly-47	Py	0.96	2.81	0.14	n.a.	482.0	1.13	38.69	2.17	

b.d.—below detection, n.a.—not analyzed. ^{40}Ar* is the excess argon without ^{40}Ar atmosphere; He_{mantle} (%) = $[(^{3}He/^{4}He)_{sample} - (^{3}He/^{4}He)_{crust}]/[(^{3}He/^{4}He)_{mantle} - (^{3}He/^{4}He)_{crust}] \times 100$, adopting 0.01 Ra as crustal He, and 6 Ra as mantle He; ^{40}Ar* (%) = $((^{40}Ar/^{36}Ar)_{Sample} - 298)/(^{40}Ar/^{36}Ar)_{Sample} \times 100$; ^{40}Ar*/^{4}He = $(^{40}Ar - 298 \times {}^{36}Ar)/^{4}He$.

5.2. S Isotopic Compositions

Sulfur isotope data of ore sulfides are presented in Table 3 and illustrated graphically in Figure 10. The $\delta^{34}S$ values of five pyrite samples from the Longquanzhan gold deposit are mostly in the range of 0.9–2.3‰ with an average of 1.5‰. Integrating with three pyrite samples analyzed by [43], the $\delta^{34}S$ values still exhibit a quite narrow range of 0.9–4.4‰. Overall, sulfur isotopic compositions show a pronounced normal distribution and are characterized by slight ^{34}S enrichment (Figure 10). The narrow range of $\delta^{34}S$ values are with a standard deviation of 1.2.

Table 3. Sulfur isotopic compositions of sulfides from the Longquanzhan and Nanxiaoyao gold deposits in the Tan-Lu fault zone.

Sample Locations	Sample No.	Measured Minerals	$\delta^{34}S$(‰)	Data Source
Longquanzhan gold deposit	NJ-6	Py	1.0	This study
	NJ-9	Py	1.9	
	NJ-20	Py	1.6	
	NJ-22	Py	2.3	
	NJ-24	Py	0.9	
Nanxiaoyao gold deposit	Sly-64	Py	2.7	[43]
Longquanzhan gold deposit	Zk5201-H64	Py	4.4	
	Sly-47	Py	3.3	

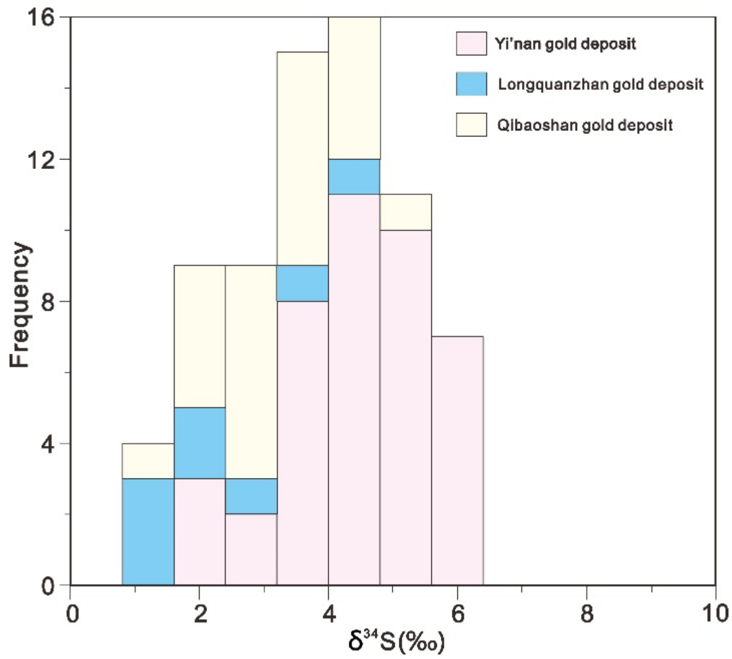

Figure 10. Histogram of sulfur isotopic compositions ($\delta^{34}S$) of sulfides from the Longquanzhan gold deposit and the Luxi-Jiaodong gold ore system. The sulfur isotopic data for the Yi'nan and Qibaoshan gold deposits are from [4,48,49].

6. Discussion

6.1. Sources of Ore-Forming Fluids and Metals

Previous studies have confirmed that different earth reservoirs possess strong different noble gas isotopic compositions [50–53]. Potential reservoirs include: 1) air-saturated water (ASW, i.e., meteoric or marine water), with $^3He/^4He$ ratio of 1.39 × 10^{-6} (1 Ra) and $^{40}Ar/^{36}Ar$ ratio of 298; 2) mantle-derived fluids, with high ^3He and low ^{36}Ar contents, $^3He/^4He$ = 6–9 Ra and $^{40}Ar/^{36}Ar$ = 30,000–40,000; and 3) K-rich crust-derived fluids, with $^3He/^4He$ ratio of 0.01–0.05 Ra and $^{40}Ar/^{36}Ar$ = ~100,000 [54]. Before noble gas can be used to determine sources of mineralizing fluids, the role of noble gas loss/diffusion and in situ radiogenic, nucleogenic and cosmogenic components, needs to be determined. All pyrite samples analyzed in this study were obtained from underground tunnels and drill cores, so cosmogenic He as a source of high $^3He/^4He$ can be ruled out. As a suitable noble gas carrier, He and Ar diffusion coefficients of fluid inclusions in pyrite are very low [50]. Therefore, He and Ar diffusive loss from fluid inclusions for He–Ar isotope variations are negligible. Besides, the radiogenic ^3He can also be ignored considering the lack of Li-bearing minerals in pyrite samples [55,56]. Additionally, the amount of He in the atmosphere is extremely low and has limited influence on the He abundances and isotopic compositions of most crustal fluids [57]. Thus, all He–Ar isotopic compositions measured in this study are representative of the compositions of primary fluid inclusions trapped in pyrite.

The $^3He/^4He$ ratios of fluid inclusions in pyrite from the Longquanzhan gold deposit are between 0.14 and 0.78 Ra, with an average of 0.3 Ra, which is higher than crustal values (0.01–0.05 Ra) but lower than those of mantle (6–9 Ra). Furthermore, in the ^4He vs. ^3He diagram, all data points are plotted in the transition zone between mantle and crustal helium isotopic compositions (Figure 8), which indicates a mixing source between crustal and mantle-derived components for the ore-forming fluids. According to the crust-mantle binary mixing model [58], the calculated results show that the percentage of mantle-derived helium in the ore fluids of the Longquanzhan deposit ranges from 2.17%–12.85% (average 4.78%), reflecting that the ore-forming fluids were mainly derived from crust source, but mixed with minor mantle components in the magmatic source. Meanwhile, this also resembles those of the Qibaoshan (3.02–3.07%) and Yi'nan (1.82–18.45%) gold deposits, indicating their magmatic origin and confirming the minor mantle contributions (Table 2).

Previous studies have shown that the $^{40}Ar^*/^4He$ ratios of sub-continental lithospheric mantle (SCLM) fluids are normally in the range of 0.33–0.56 [52,53,59], and the average value for the crust is about 0.2 [46]. However, the calculated $^{40}Ar^*/^4He$ ratios for the enriched mantle in the Shandong area range from 4.76 to 5.67, which is significantly higher than the normal SCLM [12]. The $^{40}Ar^*/^4He$ ratios of the Longquanzhan ore fluids are between 0.03 and 1.13, lower than that of magmatic end-member of Jiaodong (Table 2; Figure 9b) [12]. This gives further proof for the above interpretation of a crust-dominated source for the ore fluids.

The $^{40}Ar/^{36}Ar$ ratios of pyrite samples from the Longquanzhan gold deposit vary from 482 to 1811 with an average of 1078, which is higher than that of the air-saturated water value ($^{40}Ar/^{36}Ar$ = 298 [42]). The distinct $^{40}Ar/^{36}Ar$ values indicate a significantly higher concentration of $^{40}Ar^*$(radiogenic ^{40}Ar), which possibly reflects a greater radiogenic ^{40}Ar component that is derived from crustal radioactive decay. The estimated radiogenic $^{40}Ar^*$ concentrations ($^{40}Ar^*$%) are 38.69%–83.68% (mean = 65.55%; Table 2), whereas the corresponding proportion of air-saturated water is 16.32–61.31% (mean = 34.45%), thus indicating meteoric water involvement, as well (Figure 9a). This resembles the He–Ar isotopic characteristics of the Qibaoshan gold deposit, with the $^{40}Ar^*$ values of 0.67–64.92% (Table 2). Additionally, air-saturated water involvement in the Longquanhan gold mineralization is also supported by the result of previous H–O isotopic studies [43]. The Longquanzhan gold deposit has high $^{40}Ar/^{36}Ar$ (482–1811) and $^{40}Ar^*/^4He$ (0.27–1.13) ratios, but relatively lower $^3He/^4He$ values (Figures 9b and 11a). This could probably reflect that the greater radiogenic ^{40}Ar component in the Longquanzhan is unlikely to be the isotopic characteristics of the source (i.e., deep magma). It is noteworthy that K-bearing minerals are abundant in the host monzogranite (Figure 3). Radiogenic ^{40}Ar can be accumulated from K decay in these K-bearing minerals. Hence, a plausible explanation is that fluids have inherited high radiogenic ^{40}Ar concentrations from wall rocks during interacting process. The data points in $^{40}Ar/^{36}Ar$ vs. R/Ra diagram and $^{40}Ar^*/^4He$ vs. R/Ra diagram (Figure 9) present the same distribution characteristics, that is, all the analytical data fall between the fields for crustal and mantle fluids.

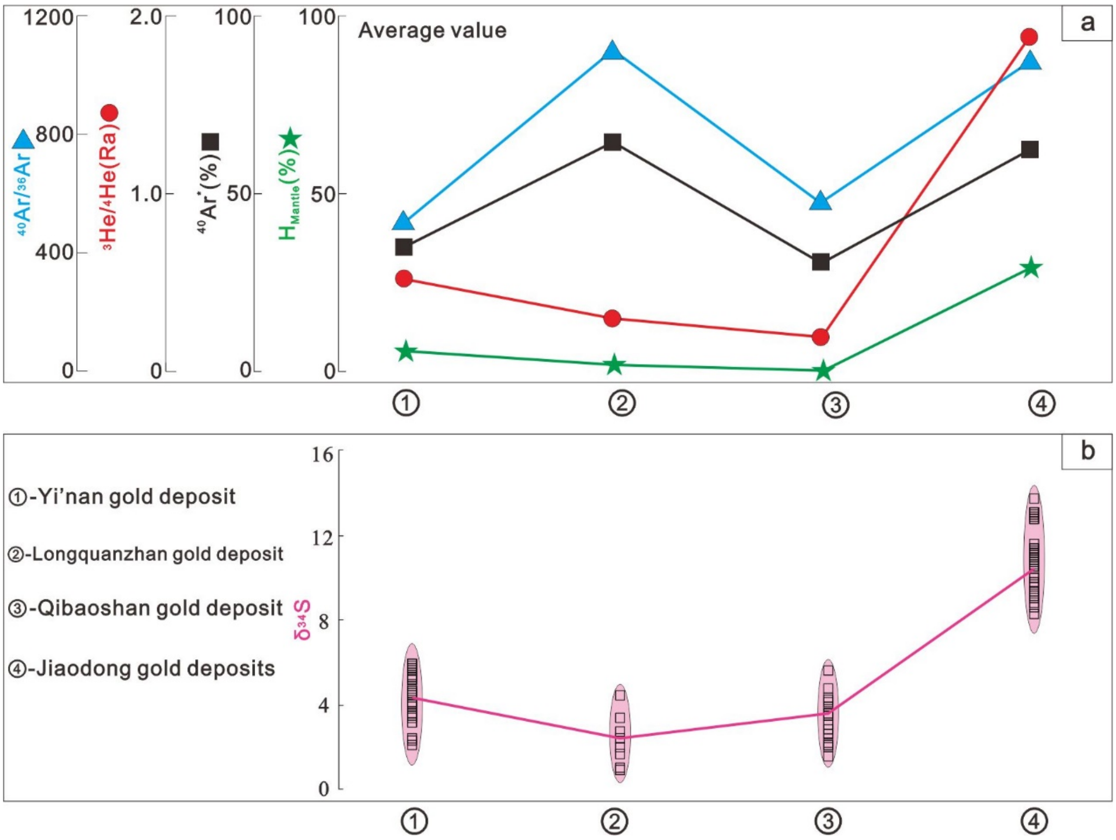

Figure 11. The sulfur, helium, and argon isotopic compositions along the section from the Luxi to Jiaodong gold ore systems. The sulfur isotopic data for the typical gold deposits in the Jiaodong area are from [4,7,48,49].

The $\delta^{34}S$ values of the Longquanzhan gold deposit range from 0.9‰ to 4.4‰ with an average of 1.5‰ (Table 3; Figure 10), which are close to the magmatic values (0 ± 2‰, [60]) and consistent with those of magmatic sulfides from the 21°N East Pacific Rise and Mid-Atlantic Ridge (+1‰ to +3.5‰, [57]). A comparison of sulfur isotopic compositions also shows that the $\delta^{34}S$ values of the Longquanzhan gold deposit reported here are compatible with those of the Qibaoshan (1.53–5.6‰, [48]) and Yi'nan (2–5.89‰, [49]) gold deposits (Table 3; Figures 10 and 11b), but lower than those of the Jiaodong gold deposits, further indicating their magmatic origin and minor mantle contributions. This is because that the higher $\delta^{34}S$ values in Jiaodong seem to be related to degassing of mantle wedge metasomatized by slab fluids [61]. Previous studies of lead isotopes of pyrites from the Longquanzhan gold deposit have indicated a dominant role of the lower crust in providing lead and metals in the ore system [43]. This is also supported by the high initial $^{87}Sr/^{86}Sr$ ratios of gold-bearing pyrite (0.71409 ± 0.00001) from the main gold mineralization stage [21]. Thus, the magmatic source should be crustal level and as the result of crust partial melting, with minor mantle melt input.

In summary, the noble gas and sulfur isotope evidence for the Longquanzhan gold deposit reveals a significant contribution of crustal components with minor mantle contributions in the gold mineralization-related hybrid magmatic source. Air-saturated water was involved in the hydrothermal system during the magmatic fluids ascending or at shallow crustal deposit site.

6.2. Ore Genesis and Geodynamic Setting

The mineralization difference across the Shandong Province has drawn much attention over the past decades, since the Luxi and the Yi-Shu belt only host several small-middle gold deposits [1,7,21] (Figure 1). Extensive gold mineralization occurring in the Jiaodong Peninsula has been proved to be the result of sequential geological processes including the

NCC decratonization, astheno-spheric upwelling, and mantle-crust melt mixing [1–3,5–11]. This is consistent with the fact that numerous coeval mafic-felsic dikes and granitoid displaying mantle-crust mixing features are spatially and temporally associated with gold ore formation [17]. Previous studies have also indicated that the Tan-Lu fault zone is an extensive thinning zone during the destruction of NCC [22,29,36]. Compared with inner craton, the magmatic activities in the Tan-Lu fault zone have a relatively long duration and a later terminal time, which is supported by the late Cretaceous mafic dikes (ca. 95–87 Ma, [15]), sodic volcanic rocks (106–97 Ma, [22,29]) within Yi-Shu fault zone, and Chaohu A-type granites (ca. 108–103 Ma), bimodal volcanism (ca. 125–93 Ma) in the south section of the Tan-Lu fault zone [62]. These magmatic rocks reveal that older enriched lithospheric mantle beneath the Yi-Shu belt had been continuously eroded by astheno-spheric upwelling in the Late Cretaceous [22,29]. This process may provide heat along with some decompression to trigger melting of the overlying crust (due to persistently ascending of isotherm plane), well before astheno-spheric melts eventually reached the surface. This interpretation is consistent with the fact that, from early to late, the ancient crustal components involved in volcanic and magmatic rocks gradually increased, and magma sources became shallower [22,62]. The late Cretaceous permanent magmatic activities, triggered by the intensely astheno-spheric upwelling, are contemporaneous with Longquanzhan and other gold mineralization, indicating that they might be genetically related. This speculation is supported by characteristics of He–Ar–S isotopic compositions from the Longquanzhan gold deposit which indicates that the ore-forming fluids were mainly derived from the crust but mixed with minor mantle components (Figures 8–11).

Our interpretation may also explain much of the gold ore formation near the Yi-Shu fault belt, exemplified by the Yi'nan and the Qibaoshan, which exhibit much disparity with the Jiaodong gold deposits (Figure 11). They have consistent noble gas and sulfur isotopic compositions with the Longquanzhan deposit, except for higher argon contents, also indicating a crust-dominated origin. First of all, these deposits are located close to or within the Yi-Shu fault belt (Figure 1). Previous studies have shown that the tectonic setting during the ore formation had changed from regional rifting to intensively extension [20,21,63]. Thus, we suggest that tectonic extension (probably elevated geothermal temperature due to mantle underplating) induced the decompression melting of lower to middle crust [1], and these crust-derived magmas, with minor mantle input, finally resulted in the formation of these gold deposits. Our previous studies also showed that the mine Au reserve is positively correlated with the proportion of mantle-derived He in the ore-forming fluids [12]. This reasonably explains the limited scale and intensity of gold mineralization in the Luxi and the Yi-Shu belt (Figure 1).

7. Conclusions

Noble gas and sulfur isotopic data from the Longquanzhan and adjacent gold deposits lead us to the following main conclusions:

(1) The ore-forming fluids are derived from a magma mixing source in which the crustal melt is dominated. The magmatic fluids are dominated by crust-derived components with minor mantle contributions. During ascending of the magmatic fluids or at shallow crustal deposit site, air-saturated water is also involved in the hydrothermal system.

(2) The mixed crust-mantle origin for the Longquanzhan in the Yi-Shu fault zone is genetically associated with the NCC destruction in the Late Cretaceous. Constantly uplifting of the asthenosphere surface and persistently ascending of isotherm plane leads to the generation of the crustal level magma source for gold mineralization.

(3) Gold ore formation within or near the Yi-Shu fault zone may share a similar extensional regime where older enriched lithospheric mantle had been continuously eroded by astheno-spheric upwelling. Hence, partial melting of the overlying crust may be the main mechanism for the formation of ore fluids.

Author Contributions: Conceptualization, C.L. and W.S.; methodology, J.W.; formal analysis, H.L.; investigation, C.L., W.S., J.D. and J.Z.; resources, A.F. and Y.Y.; data curation, H.L.; writing—original draft preparation, C.L.; writing—review and editing, W.S. and J.T.; supervision, W.S.; project administration, W.S. and J.T.; funding acquisition, W.S. and J.T. All authors have read and agreed to the published version of the manuscript.

Funding: This research was funded by the National Key R&D Program of China (Grant No. 2016YFC0600105), Natural National Science Foundation of China (41772071), and Fundamental Research Funds for the Central Universities, China University of Geosciences (Wuhan) (CUGL17043 and CUG180609).

Data Availability Statement: Data are contained within the article and Tables 1–3.

Acknowledgments: The manuscript significantly benefited from the reviews by two anonymous reviewers. Suggestions from Lebing Fu helped to improve the manuscript during revision. We also thank the Shandong Institute of Geological Survey for the assistance during the fieldwork.

Conflicts of Interest: The authors declare no conflict of interest.

References

1. Guo, P.; Santosh, M.; Li, S.R. Geodynamics of gold metallogeny in the Shandong Province, NE China: An integrated geological, geophysical and geochemical perspective. *Gondwana Res.* **2013**, *24*, 1172–1202. [CrossRef]
2. Li, S.R.; Santosh, M. Metallogeny and craton destruction: Records from the North China Craton. *Ore Geol. Rev.* **2014**, *56*, 376–414. [CrossRef]
3. Goldfarb, R.J.; Santosh, M. The dilemma of the Jiaodong gold deposits: Are they unique? *Geosci. Front.* **2014**, *5*, 139–153. [CrossRef]
4. Liu, Y.; Santosh, M.; Li, S.R.; Guo, P. Stable isotope geochemistry and Re-Os ages of the Yinan gold deposit, Shandong Province, northeastern China. *Int. Geol. Rev.* **2014**, *56*, 695–710. [CrossRef]
5. Xu, G.Z.; Zhou, R.; Wang, Y.F.; She, H.Q.; Li, B.; Du, B.M.; Song, M.C. The intrinsic factors caused the significant differences in Mesozoic mineralization between Jiaodong and Luxi areas. *Geoscience* **2002**, *16*, 9–17, (In Chinese with English Abstract).
6. Li, L.; Santosh, M.; Li, S.R. The 'Jiaodong type' gold deposits: Characteristics, origin and prospecting. *Ore Geol. Rev.* **2015**, *65*, 589–611. [CrossRef]
7. Mao, J.W.; Wang, Y.T.; Li, H.M.; Pirajno, F.; Zhang, C.Q.; Wang, R.T. The relationship of mantle-derived fluids to gold metallogenesis in the Jiaodong Peninsula: Evidence from D-O-C-S isotope systematics. *Ore Geol. Rev.* **2008**, *33*, 361–381. [CrossRef]
8. Yang, J.H.; Wu, F.Y.; Wilde, S.A. A review of the geodynamic setting of large-scale Late Mesozoic gold mineralization in the North China Craton: An association with lithospheric thinning. *Ore Geol. Rev.* **2003**, *23*, 125–152. [CrossRef]
9. Li, S.R.; Santosh, M. Geodynamics of heterogeneous gold mineralization in the North China Craton and its relationship to lithospheric destruction. *Gondwana Res.* **2017**, *50*, 267–292. [CrossRef]
10. Zhu, R.X.; Fan, H.R.; Li, J.W.; Meng, Q.R.; Li, S.R.; Zeng, Q.D. Decratonic gold deposits. *Sci. China Earth Sci.* **2015**, *58*, 1523–1537. [CrossRef]
11. Li, J.-W.; Bi, S.-J.; Selby, D.; Chen, L.; Vasconcelos, P.M.; Thiede, D.; Zhou, M.-F.; Zhao, X.-F.; Li, Z.-K.; Qiu, H.-N. Giant Mesozoic gold provinces related to the destruction of the North China Craton. *Earth Planet. Sci. Lett.* **2012**, *349–350*, 26–37. [CrossRef]
12. Tan, J.; Wei, J.H.; He, H.Y.; Su, F.; Li, Y.J.; Fu, L.B.; Zhao, S.Q.; Xiao, G.L.; Zhang, F.; Xu, J.F.; et al. Noble gases in pyrites from the Guocheng-Liaoshang gold belt in the Jiaodong province: Evidence for a mantle source of gold. *Chem. Geol.* **2018**, *480*, 105–115. [CrossRef]
13. Chai, P.; Hou, Z.Q.; Zhang, Z.Y. Geology, fluid inclusion and stable isotope constraints on the fluid evolution and resource potential of the Xiadian gold deposit, Jiaodong Peninsula. *Resour. Geol.* **2017**, *67*, 341–359. [CrossRef]
14. Gao, S.; Rudnick, R.L.; Yuan, H.L.; Liu, X.M.; Liu, Y.S.; Xu, W.L.; Ling, W.L.; Ayers, J.; Wang, X.C.; Wang, Q.H. Recycling lower continental crust in the North China Craton. *Nature* **2004**, *432*, 892–897. [CrossRef] [PubMed]
15. Cai, Y.C.; Fan, H.R.; Santosh, M.; Liu, X.; Hu, F.F.; Yang, K.F.; Liu, Y. Evolution of the lithospheric mantle beneath the southeastern North China Craton: Constraints from mafic dikes in the Jiaobei terrain. *Gondwana Res.* **2013**, *24*, 601–621. [CrossRef]
16. Zhang, H.F. Destruction of ancient lower crust through magma underplating beneath Jiaodong Peninsula, North China Craton: U-Pb and Hf isotopic evidence from granulite xenoliths. *Gondwana Res.* **2012**, *21*, 281–292. [CrossRef]
17. Tan, J.; Wei, J.H.; Audétat, A.; Pettke, T. Source of metals in the Guocheng gold deposit, Jiaodong Peninsula, North China Craton: Link to early Cretaceous mafic magmatism originating from Paleoproterozoic metasomatized lithospheric mantle. *Ore Geol. Rev.* **2012**, *48*, 70–87. [CrossRef]
18. Ma, L.; Jiang, S.Y.; Hofmann, A.W.; Dai, B.Z.; Hou, M.L.; Zhao, K.D.; Chen, L.H.; Li, J.W.; Jiang, Y.H. Lithospheric and asthenospheric sources of lamprophyres in the Jiaodong Peninsula: A consequence of rapid lithospheric thinning beneath the North China Craton? *Geochim. Cosmochim. Acta* **2014**, *124*, 250–271. [CrossRef]
19. Ma, L.; Jiang, S.Y.; Hofmann, A.W.; Xu, Y.G.; Dai, B.Z.; Hou, M.L. Rapid lithospheric thinning of the North China Craton: New evidence from cretaceous mafic dikes in the Jiaodong Peninsula. *Chem. Geol.* **2016**, *432*, 1–15. [CrossRef]

20. Deng, J.; Liu, X.; Wang, Q.; Dilek, Y.; Liang, Y. Isotopic characterization and petrogenetic modeling of Early Cretaceous mafic diking-Lithospheric extension in the North China craton, eastern Asia. *Geol. Soc. Am. Bull.* **2017**, *129*, 1379–1407. [CrossRef]
21. Shi, W.J.; Wei, J.H.; Tan, J.; Li, Y.J.; Fu, L.B.; Li, H.; Zhao, S.Q.; Tian, N. Late Early Cretaceous gold mineralization in Tan-Lu fault zone: Evidence from Rb-Sr isotopic dating of pyrite from Longquanzhan gold deposit. *Earth Sci. J. China U Geosci.* **2014**, *39*, 325–340, (In Chinese with English Abstract). [CrossRef]
22. Li, Y.L.; Qiu, J.S.; Liu, L. Geochronology and geochemistry of sodic volcanic rocks from Shenquan in Tancheng County, Shandong Province: Implications for unravelling the nature of mantle source and petrogenesis. *Acta Petrol. Miner.* **2012**, *31*, 783–798, (In Chinese with English Abstract).
23. Wang, X.F.; Li, Z.J.; Chen, B.L. *Tan-Lu Fault Belt*; Geology Publishing House: Wuhan, China, 2000; pp. 12–308. (In Chinese)
24. Wang, R.; Shi, W.; Zhang, X.; Tang, D.; Chen, H.; Xu, Q.; Xu, Z. Magmatic Activity Characteristics and Its Coupling Relationship with Regional Tectonics in the Eastern Depression of North Yellow Sea Basin, Eastern China. *Earth Sci. J. China U Geosci.* **2017**, *42*, 587–600, (In Chinese with English Abstract). [CrossRef]
25. Zhang, J.; Li, W.; Wu, Z.P.; Li, C.R.; Yang, B.; Zhang, X.Q. Structural Characteristics of Tan-Lu Fault Zone in South Area of Bohai Sea and Its Control on Basin Structure. *Earth Sci. J. China U Geosci.* **2017**, *42*, 1549–1564, (In Chinese with English Abstract). [CrossRef]
26. Shi, W.J. The Late Mesozoic Tectonic-Magmatic Evolution Process in the Yishu Fault Zone and Adjacent Regions, Shandong Province: Implication for Gold Mineralization. Ph.D. Thesis, China University of Geosciences, Wuhan, Hubei, 2014. (In Chinese with English Abstract).
27. Shen, Q.H.; Zhang, Z.Q.; Xu, H.F. Study on the isochron age in the Archean granulite terrains of Yishui, Shandong Province. *Acta Geol. Sin.* **1994**, *1*, 17–19, (In Chinese with English Abstract).
28. Wang, S.J.; Wan, Y.S.; Song, Z.Y.; Yang, E.X.; Wang, W.; Dong, C.Y.; Liu, L. Stratigraphic division and formation era of Taishan Group in Luxi area: Evidence of zircon SHRIMP U-Pb dating. Miner. *Resour. Geol.* **2012**, *28*, 15–23, (In Chinese with English Abstract).
29. Qiu, J.S.; Liu, L.; Li, Y.L. Geochronology and geochemistry of potassic and sodic volcanic rocks in Tangtou basin, Shandong Province: Implications for lithospheric thinning beneath the North China Craton. *Acta Petrol. Sin.* **2012**, *28*, 1044–1056, (In Chinese with English Abstract).
30. Liu, D.Y.; Jian, P.; Kröne, A.; Xu, S.T. Dating of prograde metamorphic events deciphered from episodic zircon growth in rocks of the Dabie–Sulu UHP complex, China. *Earth Planet. Sci. Lett.* **2006**, *250*, 650–666. [CrossRef]
31. Su, S.G.; Zhou, X.R.; Gu, D.L. Characteristics, ages and geneses of charnockites in Yishui area, Shandong Province. *Earth Sci. J. China U Geosci.* **1999**, *24*, 58–62, (In Chinese with English Abstract).
32. Shen, Q.H.; Zhao, Z.R.; Song, B.; Song, H.X. Geology, petrochemistry and SHRIMP zircon U-Pb dating of the Mashan and Xueshan granitoids in Yishui County, Shandong Province. *Geol. Rev.* **2007**, *53*, 180–186, (In Chinese with English Abstract). [CrossRef]
33. Zhao, Z.R.; Song, H.X.; Shen, Q.H.; Song, B. Geological and geochemical characteristics and SHRIMP U-Pb zircon dating of the Yinglingshan granite and its xenoliths in Yishui County, Shandong, China. *Geol. Bull. China* **2008**, *27*, 1551–1558, (In Chinese with English Abstract).
34. Jahn, B.M.; Liu, D.Y.; Wan, Y.S.; Song, B.; Wu, J.S. Archean crustal evolution of the Jiaodong Peninsula, China, as revealed by zircon SHRIMP geochronology, elemental and Nd-isotope geochemistry. *Am. J. Sci.* **2008**, *308*, 232–269. [CrossRef]
35. Lan, T.G.; Fan, H.R.; Santosh, M.; Hu, F.F.; Yang, K.F.; Yang, Y.H.; Liu, Y.S. Early Jurassic high-K calc-alkaline and shoshonitic rocks from the Tongshi intrusive complex, eastern North China Craton: Implication for crust-mantle interaction and post-collisional magmatism. *Lithos* **2012**, *140–141*, 183–199. [CrossRef]
36. Gu, H.O.; Xiao, Y.; Santosh, M.; Li, W.Y.; Yang, X.; Pack, A.; Hou, Z. Spatial and temporal distribution of Mesozoic adakitic rocks along the Tan-Lu fault, Eastern China: Constraints on the initiation of lithospheric thinning. *Lithos* **2013**, *177*, 352–365. [CrossRef]
37. Wang, Y.; Fan, H.R.; Hu, F.F.; Lan, T.G. Ore-forming fluids and metallogenesis of the Qibaoshan Cu-Au deposit in the Wulian County, Shandong Province, China. *Acta Petrol. Sin.* **2008**, *24*, 2029–2036, (In Chinese with English Abstract).
38. Baptiste, P.J.; Fouquet, Y. Abundance and isotopic composition of helium in hydrothermal sulfides from the East Pacific Rise at 13 °N. *Geochim. Cosmochim. Acta* **1996**, *60*, 87–93. [CrossRef]
39. Ye, X.R.; Tao, M.X.; Yu, C.A.; Zhang, M.J. Helium and neon isotopic compositions in the ophiolites from the Yarlung Zangbo River, southwestern China: The information from deep mantle. *Sci. China Ser. D Earth Sci.* **2007**, *50*, 801–812. [CrossRef]
40. Tan, J.; Wei, J.H.; Li, Y.J.; Fu, L.B.; Li, H.M.; Shi, W.J.; Tian, N. Origin and geo- dynamic significance of fault-hosted massive sulfide gold deposits from the Guocheng-Liaoshang metallogenic belt, easternJiaodong Peninsula: Rb-Sr dating, and H-O-S-Pb isotopic constraints. *Ore Geol. Rev.* **2015**, *65*, 687–700. [CrossRef]
41. Mamyrin, B.A.; Tolstikhin, I.N. *Helium Isotopes in Nature*, 1st ed.; Amsterdam Press: Amsterdam, The Netherlands, 1984; 237p.
42. Mark, D.F.; Stuart, F.M.; de Podesta, M. New high-precision measurements of the isotopic composition of atmospheric argon. *Geochim. Cosmochim. Acta* **2011**, *75*, 7494–7501. [CrossRef]
43. Hu, H.B.; Sun, A.Q.; Niu, S.Y.; Wang, B.D.; Li, Y.P. Helium and argon isotopic com positions of the Longquanzhan gold deposit in the Yi-Shu fault zone and their geological implications. *Chin. J. Geochem.* **2007**, *26*, 46–51. [CrossRef]
44. Zhang, L.C.; Zhou, X.H.; Ding, S.J. Mantle-derived fluids involved in large-scale gold mineralization, Jiaodong district, China: Constraints provided by the He-Ar and H-O isotopic systems. *Int. Geol. Rev.* **2008**, *50*, 472–482. [CrossRef]

45. Li, J.; Song, M.C.; Liang, J.L.; Jiang, M.Y.; Li, S.Y.; Ding, Z.J.; Su, F. Source of ore-forming fluids of the Jiaojia deeply seated gold deposit: Evidences from trace elements and sulfur-helium-argon isotopes of pyrite. *Acta Petrol. Sin.* **2020**, *36*, 297–313, (In Chinese with English Abstract). [CrossRef]
46. Torgersen, T.; Kennedy, B.M.; Hiyagon, H.; Chiou, K.Y.; Reynolds, J.H.; Clarke, W.B. Argon accumulation and the crustal degassing flux of 40Ar in the Great Artesian Basin, Australia. *Earth Planet. Sci. Lett.* **1989**, *92*, 43–56. [CrossRef]
47. Winckler, G.; Aeschbach-Hertig, W.; Kipfer, R.; Botz, R.; Rubel, A.P.; Bayer, R.; Stoffers, P. Constraints on origin and evolution of Red Sea brines from helium and argon isotopes. *Earth Planet. Sci. Lett.* **2001**, *184*, 671–683. [CrossRef]
48. Qiu, J.S.; Wang, D.Z.; Ren, Q.J.; Zhang, Z.Z. Physical-chemical conditions for mineralization of the Qibaoshan gold-copper deposit and its metallogeny in Wulian country, Shandong Province. *Miner. Resour. Geol.* **1994**, *39*, 12–18, (In Chinese with English Abstract).
49. Li, K.; Gu, X.X.; Dong, S.Y. Isotopic geochemistry of Yinan Au-Cu-Fe deposit in Shandong Province. *Miner. Depos.* **2009**, *28*, 93–103, (In Chinese with English Abstract). [CrossRef]
50. Burnard, P.G.; Hu, R.Z.; Turner, G.; Bi, X.W. Mantle, crustal and atmospheric noble gases in Ailaoshan gold deposit, Yunnan province, China. *Geochim. Cosmochim. Acta* **1999**, *63*, 1595–1604. [CrossRef]
51. Burnard, P.G.; Polya, D.A. Importance of mantle derived fluids during granite associated hydrothermal circulation: He and Ar isotopes of ore minerals from Panasqueira. *Geochim. Cosmochim. Acta* **2004**, *68*, 1607–1615. [CrossRef]
52. Hu, R.Z.; Burnard, P.G.; Bi, X.W.; Zhou, M.F.; Pen, J.T.; Su, W.C.; Wu, K.X. Helium and argon isotope geochemistry of alkaline intrusion-associated gold and copper deposits along the Red River–Jinshajiang fault belt, SW China. *Chem. Geol.* **2004**, *203*, 305–317. [CrossRef]
53. Hu, R.Z.; Burnard, P.G.; Bi, X.W.; Zhou, M.F.; Pen, J.T.; Su, W.C.; Zhao, J.H. Mantle-derived gaseous components in ore-forming fluids of the Xiangshan uranium deposit, Jiangxi province, China: Evidence from He, Ar and C isotopes. *Chem. Geol.* **2009**, *266*, 86–95. [CrossRef]
54. Kendrick, M.A.; Burnard, P. Noble gases and halogens in fluid inclusions: A journey through the Earth's crust. In *The Noble Gases as Geochemical Tracers, Advances in Isotope Geochemistry*; Burnard, P., Ed.; Springer: Berlin/Heidelberg, Germany, 2013; pp. 319–369. [CrossRef]
55. Stuart, F.M.; Burnard, P.G.; Taylor, R.P. Resolving mantle and crustal contributions to ancient hydrothermal fluids: He-Ar isotopes in fluid inclusions from Dae Hwa W-Mo mineralisation, South Korea. *Geochim. Cosmochim. Acta* **1995**, *59*, 4663–4673. [CrossRef]
56. Ballentine, C.J.; Burnard, P.G. Production, release and transport of noble gases in the continental crust. *Rev. Mineral. Geochem.* **2002**, *47*, 481–538. [CrossRef]
57. Stuart, F.M.; Turner, G.; Duckworth, R.C.; Fallick, A.E. Helium isotopes as tracers of trapped hydrothermal fluids in ocean-floor sulfides. *Geology* **1994**, *22*, 823–826. [CrossRef]
58. Xu, S.; Nakai, S.; Wakita, H. Mantle-derived noble gases in natural gases from Songliao Basin, China. *Geochim. Cosmochim. Acta* **1995**, *59*, 4675–4683. [CrossRef]
59. Simmons, S.F.; Sawkins, F.J.; Schlutter, D.J. Mantle-derived helium in two Peruvian hydrothermal ore deposits. *Nature* **1987**, *329*, 429–432. [CrossRef]
60. Kyser, T.K. Stable isotopes in the continental lithospheric mantle. In *Continental Mantle*; Menzies, M., Ed.; Oxford University Press: Oxford, MS, USA, 1990; pp. 127–156.
61. Cai, Y.C.; Fan, H.R.; Santosh, M.; Hu, F.F.; Yang, K.F.; Li, X.H. Decratonic gold mineralization: Evidence from the Shangzhuang gold deposit, eastern North China Craton. *Gondwana Res.* **2018**, *54*, 1–22. [CrossRef]
62. Xie, C.L. The Late Mesozoic Magmatism along the South Segment of the Tan-Lu Fault Zone and Its Implication for Lithospheric Thinning. Ph.D. Thesis, Hefei University of Technology, Hefei, Anhui, 2008. (In Chinese with English Abstract).
63. Dai, L.Q.; Zheng, Y.F.; Zhao, Z.F. Termination time of peak decratonization in North China: Geochemical evidence from mafic igneous rocks. *Lithos* **2016**, *240*, 327–336. [CrossRef]